Communications in Physics, Vol. 29, No. 3 (2019), pp. 251-261
DOI:10.15625/0868-3166/29/3/13854

INFLUENCE OF Mn^{2+} DOPING ON STRUCTURAL PHASE TRANSFORMATION AND OPTICAL PROPERTY OF $TiO_2 : Mn^{2+}$ NANOPARTICLES

TRINH THI LOAN †AND NGUYEN NGOC LONG

Faculty of Physics, VNU University of Science, 334 Nguyen Trai, Thanh Xuan, Hanoi, Vietnam

†*E-mail:* loan.trinhthi@gmail.com

Received 31 May 2019
Accepted for publication 8 July 2019
Published 6 September 2019

Abstract. *Titanium dioxide (TiO_2) nanoparticles with various Mn^{2+}-doping concentration (from 0 to 12 mol%) were successfully synthesized by the sol–gel method using titanium tetrachloride ($TiCl_4$), and manganese II chloride tetrahydrate ($MnCl_2.4H_2O$) as precursors. The phase and crystallinity of the synthesized materials were investigated by powder X-ray diffraction pattern and Raman spectroscopy. Diffuse reflection and photoluminescence spectra were taken to investigate the absorption and emission characteristics of the synthesized samples. The results show that the anatase and rutile phases existed simultaneously in all the doping TiO_2 nanoparticles and the Mn^{2+} doping enhances anatase-rutile transformation. The Mn^{2+} contents did not affect the lattice of TiO_2 host, but affected positions of its Raman modes. The optical band gap of the TiO_2:Mn^{2+}decreases with the increase of doping concentration. Photoluminescence spectra of the TiO_2:Mn^{2+} nanopaticles showed the transitions between the bands, the transitions related to defect states and the Mn^{2+} ion doping leads to quenching the photoluminescence.*

Keywords: TiO_2:Mn^{2+}; sol-gel method; transformation; photoluminescence.

Classification numbers: 77.84.Lf; 78.55-m.

I. INTRODUCTION

Titanium dioxide (TiO_2) is a well-known material that is widely-used in various applications. Titanium dioxide nanopowder is used in mesoscopic solar cells [1], photocatalysts [2], photonic crystals [3], gas sensors [4] and thermoelectric devices [5] etc. TiO_2 occurs naturally in three crystalline forms: anatase (tetragonal), rutile (tetragonal) and brookite (orthorhombic).

Among these polymorphs, rutile and anatase have been mostly investigated. Rutile phase is stable at high-temperatures and has a band gap of 3.0 eV, anatase exists at lower temperatures with a band gap of 3.2 eV. Brookite has been rarely studied because of its complicated structure and difficulties in sample fabrication. These three phases are described as constituted by arrangements of the same building block (Ti-O_6 octahedron). In spite of the similarities in building blocks of Ti–O_6 octahedra, the electronic structures of these polymorphs are significantly different [6]. It is known that TiO_2 only absorbs ultraviolet light of solar radiation (i.e. it equals only 5% of the total solar radiation). If one can reduce the band gap of TiO_2 to the visible region, its applicability will be enhanced.

The Mn-doped TiO_2 nanocrystals have received great attention due to its enhanced sub-band-gap absorption [7] and photocatalytic efficiency [8]. In addition, ferromagnetic behavior detected in Mn-doped TiO_2 composition corresponds to the strong Mn *d*-shell contribution [9].

In this paper, we report the preparation of different content of Mn-doped TiO_2 nanoparticles by a simple sol–gel method using low-cost price chemical materials and find out the effect of Mn^{2+} on structural and optical properties of TiO_2:Mn^{2+} nanoparticles.

II. EXPERIMENT

Sol–gel method was used to prepare Mn^{2+}-doped TiO_2 samples. In a typical synthesis process appropriate amount of $MnCl_2$ was dissolved in 50 ml of ethanol alcohol solution under constant stirring for 15 min. Then 2 ml $TiCl_4$ was poured slowly drop by drop to that mixture with continued stirring and the mixed solution temperature was kept constant at 50˚C until gel was formed. The prepared gel was dried in air at 150˚C for 24 h and annealed at 600˚C for 5 h.

X-ray diffraction (XRD) was used to identify the crystalline phases and estimate the crystallite size using a Siemens D5005 Bruker, Germany diffractometer with Cu-$K_{\alpha 1}$ irradiation ($\lambda =$ 1.54056 Å). Raman spectra were measured using LabRam HR800, Horiba spectrometer with 632.8 nm excitation. Nova Nano SEM 450, FEI field emission scanning electron microscope (FESEM) with the energy dispersive X-ray spectrometer (EDS) was used to observe the sample morphologies and elemental composition analysis. The photoluminescence (PL) spectra were measured at room temperature using a Fluorolog FL3-22 Jobin Yvon Spex, USA spectrofluorometer with a xenon lamp of 450 W being used as an excitation source.

III. RESULT AND DISCUSSION

III.1. Samples characterization

The morphologies of the 6 mol% and 12 mol% Mn-doped TiO_2 samples were observed by FESEM and are shown in Fig. 1. It can be seen that the samples comprise the near-spherical-shaped nanoparticles with the size in the range of 22–50 nm.

Typical EDS spectra of the undoped, 6 mol% Mn- and 12 mol% Mn-doped TiO_2 nanoparticles are presented in Fig. 2. As seen from this figure, the undoped sample composes of only Ti and O elements. In the 6 mol% and 12 mol% Mn^{2+}-doped TiO_2 samples, Mn element has been detected and peaks characteristic for Mn element increase in intensity with increasing amount of Mn dopant. This result indicates that the Mn^{2+} ions have incorporated into the lattice of TiO_2.

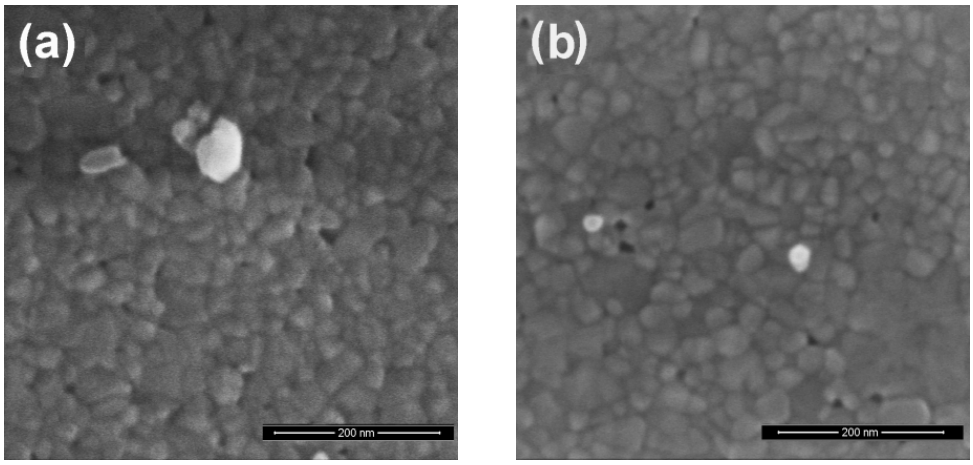

Fig. 1. The FESEM images of TiO_2:Mn^{2+}samples with different dopant concentrations: (a) 6 mol%, (b) 12 mol%, (Scale bar is 200 nm).

The XRD patterns of the Mn^{2+}-doped TiO_2 nanoparticles including Mn^{2+} contents from 0 to 12.0 mol% are shown in Fig. 3. For the undoped TiO_2 sample, nine diffraction peaks (at 2θ = 25.3˚, 36.9˚, 37.8˚, 38.8˚, 48.1˚, 54.0˚, 55.1˚, 62.7˚, and 68.8^o) were observed. These peaks correspond to the (101), (103), (004), (112), (200), (105), (211), (204), and (116) planes of anatase phase, respectively (JCPDS card: 04-0477). There is no detectable diffraction peak of rutile phase. However, for the 0.5 mol% Mn^{2+}-doped TiO_2, although the anatase phase is still prominent, a very weak peak is revealed at 2θ = 27.3˚, corresponding to the diffraction peak from (110) plane of rutile phase. With the further increase in Mn^{2+} contents, the characteristic diffraction peaks of rutile phase become predominant, while diffraction peaks of anatase phase gradually diminish in intensity.

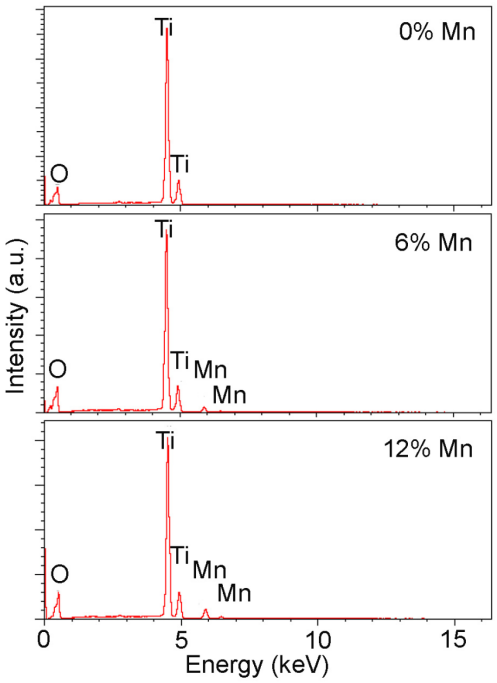

Fig. 2. The EDS spectra of TiO_2:Mn^{2+} nanoparticles with different dopant concentrations.

It is notable that no characteristic diffraction peaks for Mn or its oxide phases were present eVen for the heavily doped sample, which is indicating the high dispersion of Mn^{2+} on TiO_2 lattices. The lattice parameters of both anatase and rutile phases in the samples were calculated from the XRD patterns and are shown in Table 1.

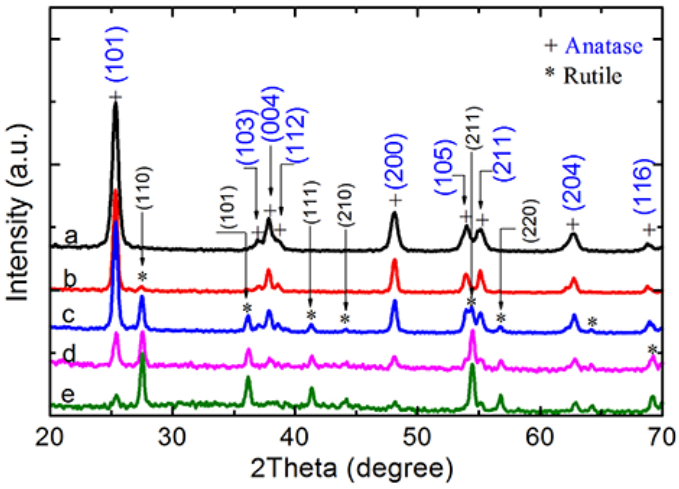

Fig. 3. XRD patterns of the TiO_2 nanoparticles doped Mn^{2+} as a function of doping concentration: a- 0 mol%, b- 0.5 mol%, c-3.0 mol%, d- 6.0 mol%, e- 12.0 mol%.

Table 1. The lattice parameters of TiO_2:Mn^{2+} nanoparticles doped with different doping concentrations.

Mn^{2+} doping concentration (mol%)	Anatase phase		Rutile phase	
	$a = b$(Å)	c (Å)	$a = b$(Å)	c (Å)
0.0	3.781 ± 0.001	9.504 ± 0.006	-	-
0.5	3.779 ± 0.001	9.519 ± 0.013	-	-
3.0	3.777 ± 0.001	9.538 ± 0.017	4.584 ± 0.001	2.953 ± 0.001
6.0	3.774 ± 0.007	9.537 ± 0.014	4.584 ± 0.001	2.951 ± 0.003
12.0	-	-	4.578 ± 0.006	2.955 ± 0.002

The result shows that the lattice parameters within the error limits remain unchanged and independent on Mn^{2+} concentration. This may be because the effective ionic radius of Mn^{2+} ion (0.67 Å) and Ti^{4+} ion (0.61 Å) in octahedral field [10] is only slightly different.

As seen from Fig. 3, when Mn^{2+} concentration is increased from 0.5 mol% to 12.0 mol%, the relative intensity of the anatase peaks with respect to rutile ones is decreased. In order to determine the quantity of anatase and rutile phases in each of the samples, the Spurr equation [11] was employed:

$$W_A(\%) = \frac{100}{1 + 1.265\left(\frac{I_R}{I_A}\right)}; \quad W_R(\%) = \frac{100}{1 + 0.8\left(\frac{I_A}{I_R}\right)},$$

where W_A and W_R are respectively the weight fractions of anatase and rutile phases ($W_R = 1 - W_A$), I_A and I_R are the integrated intensity of anatase (101) peak at $2\theta = 25.3^\circ$ and rutile (110) peak at $2\theta = 27.4^\circ$, respectively.

The results in Table 2 indicate that the Mn^{2+} doping enhances the anatase-to-rutile transformation (ART) which is good agreement with other works [12, 13]. It is well known that the ART is commonly described as a nucleation and growth process in which the rutile nuclei are formed within the anatase phase of undoped TiO_2 Indeed, when Ti^{4+} ions are replaced by Mn^{2+} ions, oxygen vacancies are formed to keep the crystal charge neutrality and with increasing Mn^{2+} ions, the concentration of oxygen vacancies at the surface of anatase grains increases, facilitating the bond rupture, leading to the structural reorganization for the formation of rutile phase. In addition, the difference in ionic radius though small, between Ti^{4+} and Mn^{2+} ions results in the lattice deformation of anatase TiO_2, and the strain energy due to the lattice deformation facilitates the ART [14, 15]. The influence of the Mn^{2+} dopant amount on the weight fractions of anatase and rutile phases, as shown in Fig. 3 and Table 2, is very clear

Table 2. Weight fractions of anatase and rutile phases in TiO_2:Mn^{2+} nanoparticles doped with different doping concentrations.

Mn^{2+} doping concentration (mol%)	W_A (%)	W_R (%)
0.0	100	0
0.5	95.0	5.0
3.0	74.5	25.3
6.0	46.1	53.8
12.0	16.0	83.9

The Raman spectroscopy is useful technique in phase structure analysis and defect identification for TiO_2. Anatase is tetragonal with the space group D_{4h}^{19} (I4/amd) and has six Raman active modes: $1A_{1g}$, $2B_{lg}$ and $3E_g$ [16]. Rutile is also tetragonal with the space group D_{4h}^{14} (P4/mnm) and has three first order Raman active modes B_{1g}, E_g and A_{1g}, along with a second-order (SO) vibrational mode [16, 17].

To affirm the above mentioned ART, Raman scattering spectra of the TiO_2:Mn^{2+} nanoparticles with different doping concentration were recorded. The results are shown in Fig. 4. As seen from the figure, the 0.5 mol% Mn^{2+}-doped TiO_2 sample exhibits five Raman active modes characteristic for anatase structure: $E_g(1)$ (141 cm^{-1}), $E_g(2)$ (194 cm^{-1}), $B_{1g}(1)$ (394 cm^{-1}), $A_{1g} + B_{1g}(2)$ (514 cm^{-1}) and $E_g(3)$ (637 cm^{-1}). No Raman active modes for rutile phase are observed. (See Fig. 4, line a). However, for 3.0 mol% Mn^{2+}-doped TiO_2 sample, beside the vibration modes of the anatase phase, the rutile-related Raman modes, E_g along with a second-order (SO) vibrational mode also appear at about 441 and 246 cm^{-1}, respectively (Fig. 4, line b). With the further increase in Mn^{2+} contents, the above rutile-related Raman modes become stronger, while the anatase-related Raman modes gradually decrease in intensity (Fig. 4, lines c and d). For 12.0 mol% Mn^{2+}-doped TiO_2 sample, the Raman modes for the anatase phase completely diminish and in Raman spectrum are observed only four Raman active modes of rutile phase, B_{1g}, E_g and A_{1g}, and SO at 141, 402, 608 and 261 cm^{-1}, respectively (Fig. 4, line e). Interestingly, no

Raman modes related to manganese oxide are detected at eVen heavily doped sample. The results are agreement with those from the XRD analysis.

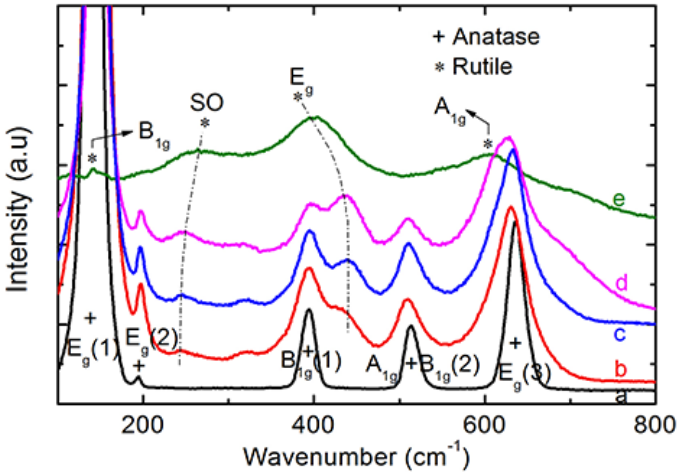

Fig. 4. Raman spectra of the TiO_2:Mn^{2+} nanoparticles as a function of doping concentration: a- 0.5 mol%, b- 3.0 mol%, c- 6.0 mol%, d- 9.0 mol%, e- 12.0 mol%.

It can be clearly seen from Fig. 4 and Table 3 that the vibration modes characterizing both anatase and rutile phases broaden and shift, when increasing Mn^{2+} content. For the anatase phase, the $E_g(1)$ and $E_g(2)$ modes broaden and shift to the higher wavenumber, but the $A_{1g}+B_{1g}(2)$ and $E_g(3)$ modes to the lower wavenumber. For the rutile phase, SO mode broadens and shifts to the higher wavenumber, while E_g mode to lower one.

Table 3. The wavenumber of some Raman modes of the anatase and rutile TiO_2:Mn^{2+} nanoparticles doped with different dopant concentrations.

Mn^{2+} doping concentration (mol%)	Anatase phase				Rutile phase	
	E_g (1) (cm^{-1})	E_g (2) (cm^{-1})	A_{1g}+B_{1g} (2) (cm^{-1})	E_g (3) (cm^{-1})	SO (cm^{-1})	E_g (cm^{-1})
0.5	140.9	194.5	514.1	637.2	-	-
3.0	145.7	197.0	509.1	631.2	246.3	440.9
6.0	144.6	196.6	510.7	632.1	246.3	440.9
9.0	145.3	197.0	509.9	627.0	250.6	436.7
12.0	-	-	-	-	260.6	402.1

As mentioned above, the incorporation of Mn^{2+} ions into leads to formation of oxygen vacancies and with increasing Mn^{2+} ions, the concentration of oxygen vacancies at the surface of

anatase grains increases, facilitating the bond rupture. This, on the one hand, favors the structural reorganization for the formation of rutile phase; the Mn^{2+} dopants, on the other hand, cause the change of the symmetry of the local structure around Mn^{2+} ions and therefore the modification in bond polarizability and strength of the O-Ti-O bonds. The result is that the Raman vibration modes broaden and shift.

III.2. Optical property

Typical diffuse reflectance spectra of Mn^{2+}-doped TiO_2 nanoparticles with Mn^{2+} contents of 0, 0.5, 1.0, 3.0 and 6.0 mol% are shown in Fig. 5(a). It is notable that the undoped TiO_2 samples are the white powders, while all the Mn-doped TiO_2 samples are pale gray ones and their color becomes deeper when the concentration of Mn increases. The diffuse reflectance spectra of the TiO_2samples doped with 9.0 and 12.0 mol% Mn^{2+} could not be measured because of their black color. As evidence from the figure, in ranging from 1.5 to 3.0 eV, with increasing Mn^{2+} dopant content, the diffuse reflectance is strongly decreased, i.e. the absorption is increased (Fig. 5(b)), which may be induced by the charge transfer transition from the 3d orbitals of Mn^{2+} ions to TiO_2 conduction band. In addition, the other reason of the increased absorption in visible region is that an amount of rutile phase is already formed in the samples with 3 and 6 mol% Mn.

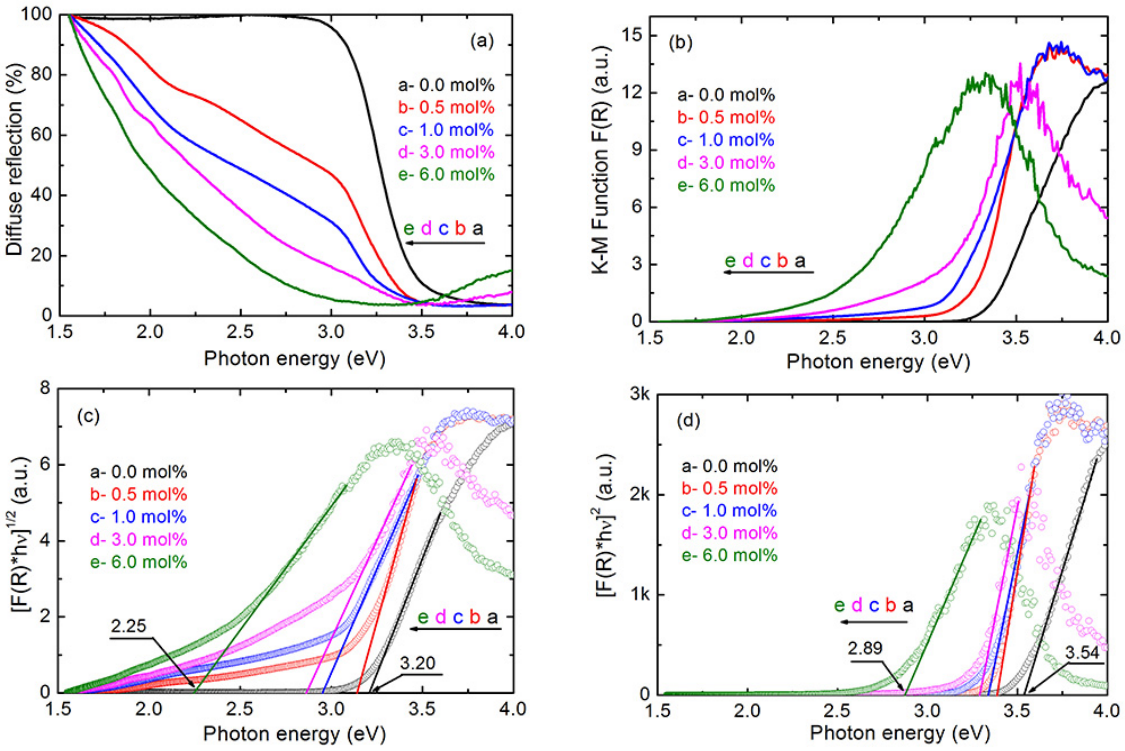

Fig. 5. (a) Diffuse reflectance spectra, (b) Kubelka-Munk functions deduced from diffuse reflectance spectra, (c) plots of $[F(R)h\nu]^{1/2}$ and (d) plots of $[F(R)h\nu]^2$ versus photon energy hν for the TiO_2:Mn^{2+} nanoparticles with different doping concentrations.

Optical band gaps E_g for the anatase TiO_2:Mn^{2+} nanopaticles with different doping concentration were determined by using Tauc equation [18]:

$$(\alpha h\nu)^n = A(h\nu - E_g)$$

where A is a constant, α is the absorption coefficient, $h\nu$ is the photon energy, n = 1/2 and 2 for the indirect and direct allowed transitions, respectively.

Fig. 5(b) shows the Kubelka-Munk functions F(R) of the TiO_2:Mn^{2+} samples obtained from the diffuse reflectance data. It can be seen that the absorption edge shifts to the visible region with increasing the Mn^{2+}concentration. The plots of $[F(R)h\nu]^{1/2}$ and $[F(R)h\nu]^2$ versus photon energy $h\nu$ are represented in Fig. 5(c) and Fig. 5(d). The band gap energies E_g for different Mn^{2+}-doped TiO_2 nanoparticles determined from Fig. 5(c) and Fig. 5(d) are given in Table 4.

Table 4. The indirect and direct band gap of the TiO2:Mn2+ nanoparticles.

Mn^{2+} dopant content (mol%)	E_g (eV)	
	Indirect transitions	Direct transitions
0	3.20	3.54
0.5	3.15	3.39
1.0	2.96	3.34
3.0	2.87	3.29
6.0	2.25	2.89

The E_g value of the undoped sample is found to be equal to 3.20 eV for the indirect band gap and 3.54 eV for the direct band gap, which are in good agreement with the calculated values reported by Daude *et al.* [19] for the indirect transition $\Gamma_3 \rightarrow X_{1b}$ (3.19 eV) and direct transition $X_{2b} \rightarrow X_{1b}$ (3.59 eV), respectively (Fig. 6). Our obtained values are also in agreement with the experimental values of 3.20 and 3.53 for TiO_2 nanoparticles reported by Reyes-Coronado *et al.* [20], and the values of 3.26 and 3.58 eV for TiO_2 nanowires reported by us [21].

It can be clearly seen from Table 4 that when the Mn^{2+} concentration is increased, both the indirect and direct band gap values are decreased. The reduction in TiO_2 band gap with increasing Mn^{2+} dopant content was reported as well in Refs. [8, 12]. It is well known that in pure TiO_2, the valence band edge is composed of O 2p states and the conduction band edge is composed of Ti 3d states [22]. Theoretical calculations indicated that the Mn^{2+} ions doped in TiO_2 can form sub-band states located between the top of valence band and the bottom of conduction band of TiO_2 [23, 24]. Additionally, the replacement of Ti^{4+} ions with Mn^{2+} ions leads to the formation of the oxygen vacancies. The oxygen vacancy states also locate in the band gap. In this case, the electrons do not directly transit to the conduction band, but via the states in the band gap. Hence, both the sub-band states of Mn^{2+} ions and oxygen vacancy states are the main reason for reducing the band gap energy of TiO_2:Mn^{2+} nanoparticles. A similar effect was also observed for the transition metal ions such as Co [21], Ni [25], Fe [26] and Cu [27] ions doped in TiO_2.

The room temperature PL spectra of undoped anatase TiO_2 nanoparticles under different excitation wavelengths are depicted in Fig. 7. The PL spectra excited at 320 and 325 nm wavelengths exhibit almost the same shape, which consists of seven peaks/shoulders at 3.13 eV (396.1

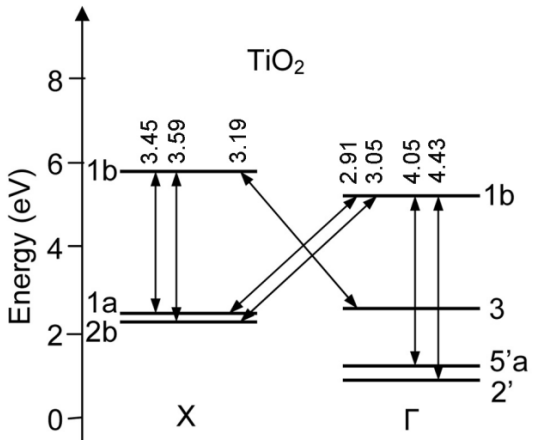

Fig. 6. Simplified energy level diagram calculated by Daude *et al.* [19], which shows the energies (in eV) for a few of the allowed indirect and direct transitions.

nm), 3.03 eV (409.2 nm), 2.84 eV (436.6 nm), 2.75 eV (450.9 nm), 2.65 eV (467.9 nm), 2.56 eV (484.3 nm) and 2.51 eV (494.0 nm).

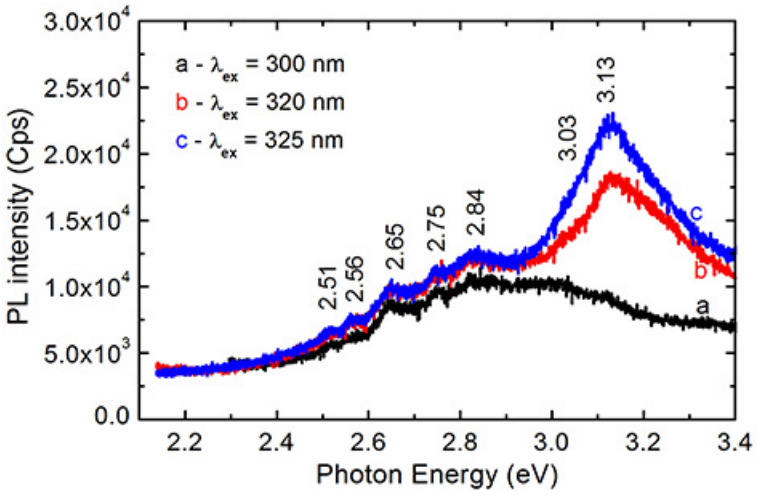

Fig. 7. The room temperature PL spectra of undoped anatase TiO_2 nanoparticles excited by different wavelengths.

The high energy peak at 3.13 eV does not appear in the PL spectrum when samples were excited with 300 nm wavelength. Generally, the PL spectra of pure anatase TiO_2 materials can be divided into three regions. The first region including the emission peaks at 3.13 and 3.03 eV can be ascribed to the near band edge emission. Namely, the peak at 3.13 eV is attributed to the $X_{1b} \rightarrow \Gamma_3$ indirect transition and the peak at 3.03 eV to $\Gamma_{1b} \rightarrow X_{1a}$(or X_{2b}) indirect transition [19]. It is noted that the transitions at 3.13 and 3.026 eV were revealed by Vos *et al.* [28]. The second region including the emission peaks at 2.84 and 2.75 eV can be assigned to the recombination of

F-centers formed from the oxygen vacancies [29,30]. Indeed, according to Serpone [31], when 2+ valence cations replace Ti^{4+} ions in TiO_2 host lattice, the formation of the oxygen vacancies (V_O) can be accompanied by the generation of F-centers, therefore, some shallow traps associated with the V_O such as F-, F^+-, F^{2+}-centers are formed, which are responsible for the emission at 2.84 and 2.75 eV. The third region including the peaks at 2.51, 2.56 and 2.65 eV, is usually assigned to the PL from TiO_2 surface defect states [30].

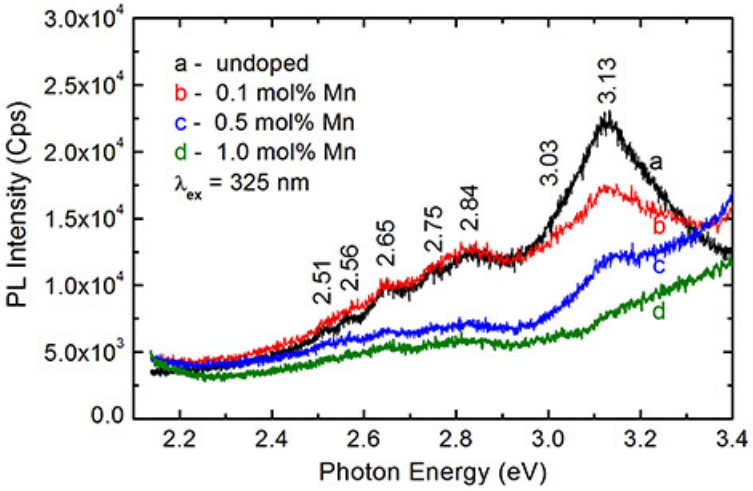

Fig. 8. The room temperature PL spectra of TiO_2:Mn^{2+} nanoparticles with different doping concentrations under excitation wavelength of 325 nm.

Fig. 8 shows the room-temprature PL spectra of TiO_2:Mn^{2+} nanoparticles with different dopingconcentration under excitation wavelength of 325 nm. It is clearly seen that Mn^{2+} ion doping leads to quenching the PL of TiO_2:Mn^{2+} nanoparticles. This may be because Mn^{2+} ions transfer excitation energy to the centers of quenching luminescence or they themselves play the role of the quenching centers.

IV. CONCLUSION

Mn^{2+} doped TiO_2 nanopaticles were successfully synthesized by simple sol-gel method. Effect of Mn^{2+} doping on the anatase-rutile transformation and optical band gap energy of the synthesized nanoparticles were investigated. The results showed that, the replacing Ti^{4+} ions with Mn^{2+}ions leaded to the phase transformation from anatase to rutile. The Mn^{2+} contents did not affect the lattice of TiO_2 host, but affected its Raman modes. The optical band gap of the TiO_2:Mn^{2+}decreased with the increase of doping concentration. Indirect and direct band gap energies of Mn^{2+}-doped TiO_2 nanoparticles were found to be in the range from 3.20 to 2.25 eV and 3.54 to 2.89 eV, respectively, when the Mn^{2+} concentration increased from 0 to 6 mol% Photoluminescence spectra of the pure anatase TiO_2 nanopaticles exhibited the transitions between the bands, the transitions related to defect states and the Mn^{2+} ion doping leaded to the luminescence quenching.

ACKNOWLEDGMENTS

This work is financially supported by VNU University of Science (Project No. TN-18-07)

REFERENCES

[1] H. Y. Yang, W. Y. Rho, S. K. Lee, S. H. Kim and Y. B. Hahn, *Nanomaterials* **9** (2019) 326.
[2] W. M. M. Mahmoud, T. Rastogi, K. Kümmerer, *Current Opinion in Green and Sustainable Chemistry* **6** (2017) 1.
[3] G. A. Ermolaev, S. E. Kushnir , N. A. Sapoletova and K. S. Napolskii, *Nanomaterials* **9** (2019) 651.
[4] Y. Seekaew , A. Wisitsoraat , D. Phokharatkul , C. Wongchoosuk, *Sensors & Actuators: B. Chemical* **279** (2019) 69.
[5] M. Mikami and K. Ozaki, *J. Phys.: Conf. Ser.* **379** (2012) 012006.
[6] S. Mugundan, B. Rajamannan, G. Viruthagiri, N. Shanmugam, R. Gobi, P. Praveen, *Appl. Nanosci.* **5** (2015) 449.
[7] V. D. Binas, K. Sambani, T. Maggos, A. Katsanaki, G. Kiriakidis, *Applied Catalysis B: Environmental* **113-114** (2012) 79.
[8] Q. R. Deng, X. H. Xia, M. L. Guo, Y. Gao, G. Shao, *Materials Letters* **65** (2011) 2051.
[9] A. Mahmood, S. M. Ramay, Y. S. Al-Zaghayer, S. Atiq, M. Saleem, W. A. A. Masary, and S. Haider, *Modern Physics Letters B* **29** (2015) 1550015.
[10] R.D. Shannon, *Acta Crystallogr. A* **32** (1976) 751.
[11] R. A. Spurr and H. Myers, *Anal. Chem.* **29** (1957) 760.
[12] L. Gomathi Devi, S. Girish Kumar, B. Narasimha Murthy, Nagaraju Kottam, *Catalysis Communications* **10** (2009) 794.
[13] D. A. H. Hanaor and C. C. Sorrell, *J. Mater. Sci.* **46** (2011) 855-874.
[14] J. Tian, H. Gao, H. Kong, P. Yang, W. Zhang and J. Chu, *Nanoscale Research Letters* **8** (2013) 533.
[15] R. R. Talavera, S. Vargas, R. A. Murillo, R. M. Campos and E. H. Poniatowski, *J. Mater. Res.* **12** (1997) 439-443.
[16] T. Ohsaka, E. Izumi and Y. Fujiki, *J. Raman Spectrosc.* **7** (1978) 321.
[17] B. Santara, P. K. Giri, K. Imakita and M. Fujii, *J. Phys. D: Appl. Phys.* **47** (2014) 215302.
[18] D. L. Wood, J. Tauc, *Phys. Rev. B* **5** (1972) 3144.
[19] N. Daude, C. Gout, C. Jouanin, *Phys. Rev. B* **15** (1977) 3229.
[20] D. Reyes-Coronado, G. Rodrıguez-Gattorno, M. E. Espinosa-Pesqueira, C. Cab, R. de Coss and G. Oskam, *Nanotechnology* **19** (2008) 145605.
[21] Trinh Thi Loan, Nguyen Ngoc Long, *J. Phys. Chem. Solids.* **124** (2019) 336.
[22] D. O. Scanlon, C. W. Dunnill, J. Buckeridge, S. A. Shevlin, A. J. Logsdail, S. M. Woodley, C. R. A. Catlow, M. J. Powell, R. G. Palgrave, I. P. Parkin, G. W. Watson, T. W. Keal, P. Sherwood, A. Walsh and A. A. Sokol, *Nat. Mater.* **12** (2013) 798.
[23] Yaqin Wang, Ruirui Zhang, Jianbao Li, Liangliang Li and Shiwei Lin, *Nanoscale Res. Lett.* **9** (2014) 46.
[24] T. Umebayashi, T. Yamaki, H. Itoh, K. Asai, *J. Phys. Chem. Solids* **63** (2002) 1909.
[25] A. K. Tripathi, M.C. Mathpal, P. Kumar, V. Agrahari, M. K. Singh, S. K. Mishra, M. M. Ahmad, A. Agarwal, *Adv. Mater. Lett.* **6** (2015) 201.
[26] M. A. Ahmed, E. E. El-Katori, Z. H. Gharni, *J. Alloy. Compd.* **553** (2013) 19.
[27] B. Choudhury, M. Dey and A. Choudhury, *Int. Nano Lett.* **3** (2013) 1.
[28] K. Vos and H. J. Krusemeyer, *Solid State Commun.* **15** (1974) 949.
[29] L. Kernazhitsky, V. Shymanovska, T. Gavrilko, V. Naumov, L. Fedorenko, V. Kshnyakin, J. Baran, *J. Lumin.* **146** (2014) 199.
[30] V. Jovic, Z.H.N. Al-Azri, W.T. Chen, D. Sun-Waterhouse, H. Idriss, G. I. N. Waterhouse, *Top. Catal.* **56** (2013) 1139.
[31] N. Serpone, *J. Phys. Chem. B* **110** (2006) 24287.